Available online at www.sciencedirect.com
SCIENCE DIRECT®
Thin Solid Films 496 (2006) 266 – 272
thin solid films
www.elsevier.com/locate/tsf

Electron energy-loss spectroscopy investigation of Y_2O_3 films on Si (001) substrate

Jingmin Zhang [a,*], Fabien Paumier [b], Thomas Höche [c], Frank Heyroth [a], Frank Syrowatka [a], Rolly J. Gaboriaud [b], Hartmut S. Leipner [a]

[a] *Martin-Luther-Universität Halle-Wittenberg, Interdisziplinäres Zentrum für, Materialwissenschaften, Hoher Weg 8, D-06120 Halle, Germany*
[b] *Université de Poitiers, Laboratoire de Métallurgie SP2MI, BP 30179 86962, Chasseneuil, Futuroscope, France*
[c] *Leibniz -Institut für Oberflächenmodifizierung, Permoserstraße 15, D-04318, Leipzig, Germany*

Received 4 January 2005; received in revised form 24 July 2005; accepted 22 August 2005
Available online 19 September 2005

Abstract

Electron energy -loss spectroscopy has been used to investigate the interface between a Y_2O_3 film and the silicon substrate. The chemical composition of the interface layer is revealed to be nearly pure amorphous SiO_2. Yttrium silicates are found at the Y_2O_3/SiO_2 interface region. The formation of the interfacial yttrium silicates has been interpreted by the direct chemical reaction between the deposited Y_2O_3 film and the SiO_2 interface layer. The Si L_{23} and O K edges of yttrium silicates (Y_2SiO_5 and $Y_2Si_2O_7$) have been calculated by the first-principle full multiple - scattering method. The theoretical results are consistent with the experimental spectra, which confirms the formation of yttrium silicates.

PACS: 79.20.Uv; 77.55.+f; 68.65.Ac; 68.37.Lp
Keywords: Electron energy loss spectroscopy(EELS); Interfaces; Scanning electron microscopy; Yttrium

1. Introduction

Silicon dioxide has been used for more than 30 years as a gate dielectric for metal-oxide-semiconductor field-effect transistors (MOSFETs). The dimensions of MOSFETs have been reduced from 10 μm in the 1970s to the present size of 90 nm. Ultrathin (1.2 nm) SiO_2 gate dielectric has been successfully implemented at today's 90 nm process node, and a 0.8 nm thick SiO_2 gate oxide has also been produced in the laboratory [1]. However, low-κ SiO_2 (permittivity $\kappa=3.9$) used as the gate dielectric almost reaches its physical limits. As metal-oxide semiconductor scales to this point, the traditional silicon dioxide gate dielectric becomes only four atomic layers thick. Tunneling current leakage and the resulting increase in power dissipation become critical issues. Further gate dielectric scaling requires high-κ materials as replacements for SiO_2. Yttrium oxide has recently attracted more attention due to its high permittivity ($\kappa=14-18$), thermal stability, and small lattice misfit with respect to silicon substrate [2]. Most investigations of the Y_2O_3/Si structure have concentrated on oxygen defects and interface reactions. In the deposited Y_2O_3 film, the major defects are oxygen vacancies. This is the reason why the deposition needs to be performed under appropriate oxygen environment in order to obtain stoichiometric Y_2O_3 films [3]. An interface layer between the deposited yttria film and the silicon substrate has been always found in previous investigations. Due to a lower permittivity, this interface layer is usually unwanted. The control and optimization of the interface layer become very important in order to substitute SiO_2 gate dielectrics.

The chemical composition of the interface layer was revealed to be SiO_x ($1\leq x\leq 2$) [4] and yttrium silicates [5–7]. These previous investigations are based on high-resolution transmission electron microscopy (HRTEM) [5,7] or X-ray diffraction [6]. More straightforward techniques need to be applied to analyze the chemical composition of the interface layer. Due to the nanosize dimension of thin films, electron energy-loss spectroscopy coupled with scanning transmission electron microscopy (STEM) is becoming an important

* Corresponding author.
E-mail addresses: zhang_jmin@pku.edu.cn (J. Zhang), leipner@cmat.uni-halle.de (H.S. Leipner).

0040-6090/$ - see front matter © 2005 Elsevier B.V. All rights reserved.
doi:10.1016/j.tsf.2005.08.337

nanoanalytical technique in these materials. Although a few papers have reported investigations of Y_2O_3/Si structures by EELS [8–10], a low energy resolution has been used, and only the Si L_{23} edges have been discussed at the interface. No systematical investigations have been carried out. That makes the formation mechanism of the interface layer still a subject to dispute. In this work, EELS/STEM has been used to investigate the interface layer and the formation of yttrium silicates.

2. Experimental details

A 220 nm thick Y_2O_3 film was deposited on a Si (001) substrate by ion beam sputtering. The deposition is described in more detail in the work of Gaboriaud et al. [3]. The substrate temperature was kept at 700 °C during the deposition on the silicon (001) substrate. The samples were investigated in the as-deposited state, without additional annealing. In order to analyze the chemical composition in the interface region, a commercial SiO_2(20 nm)/Si wafer was prepared for acquiring reference spectra. The details of specimen preparation are briefly described as follows. The Y_2O_3/Si wafer was cut into two pieces using a diamond wire saw, and then glued together face to face. An epoxy glue (M-Bond 610) with a very low viscosity was used to obtain a very thin glue layer with a thickness less than 1 μm. Due to the high speed of ion milling, the glue layer should be as thin as possible. This is important to prepare a high quality cross-section specimen with a large thin area. In the next step the sandwiched sample was glued into an alumina tube using an epoxy (G1) with a higher viscosity. The stuffing tube was successively cut into 0.5 mm thick slices which were grinded on both sides until about 80 μm thickness. In the following step single-side dimpling was performed in a Model 656 dimple grinder. The remaining thickness at the center of the dimple was estimated to about 20 μm. The other side without the dimple was finely polished. The final step was double-side ion milling with a very low incident angle (3°) in the 691 Precision Ion Polishing System. To speed up the time-consuming process, the ion milling manually started at a higher energy (3.5 keV) and ended at a lower energy (2.0 keV). A single sector mode (i.e., the specimen was thinned from only one direction) was set to prevent the very thin edge from being sputtered away by the ion beam from the opposite direction. The ion milling stopped as soon as the specimen was transparent. To minimize the spatial drift caused by charging of the sample during the STEM investigation, an amorphous carbon layer was deposited on the surface of the specimen by the High Vacuum Turbo Carbon Coater 208/C as well as the small hole was shielded from carbon coating by a thin wire.

The EEL spectra were acquired by the Gatan parallel EELS spectrometer Enfina 1000 installed on a dedicated STEM (VG HB 501 UX, Vacuum Generators) equipped with a cold field-emission gun (FEG). The STEM was operated at 100 keV. The operating pressure was $\sim 5.0 \times 10^{-9}$ mbar in the column and $\sim 3.0 \times 10^{-11}$ mbar in the FEG chamber. Both dark count readout and channel-to-channel variation in gain response were corrected by the corresponding standard procedures. The background of the spectra was removed by the AE^{-r} power-law extrapolation of the pre-edge of the core-loss edge, where A and r are constant, and E is the energy loss [11]. The energy resolution of the coupled EELS/STEM estimated by the full width at half maximum of the zero loss peak at a hole was about 0.4 eV. The probe size measured by scanning across the SiO_2/Si interface was about 0.7 nm. An entrance aperture of 2 mm was selected for collecting the inelastic electrons. The collection semi-angle was about 12 mrad. A small objective aperture with a radius of 25 μm was selected to limit the convergence semi-angle to ca. 6.5 mrad. It should be noted that the convergence angle is very critical to acquire spectra from the interface region. The fraction of the electron beam with a larger convergence angle can easily excite atoms several nanometers away from the region of interest. HRTEM images were acquired in a JEOL 4010 transmission electron microscope, which is operated at 400 keV.

3. Results and discussion

A bright-field STEM image of the Y_2O_3/Si structure investigated is shown in Fig. 1(a). An interface layer between the Y_2O_3 film and the silicon substrate is well distinguished. Similar interface layers can also be found in most of the metal oxides deposited on a Si substrate, such as Gd_2O_3 [12], La_2O_3 [13], and Ta_2O_5 [14], etc. The selected area diffraction pattern

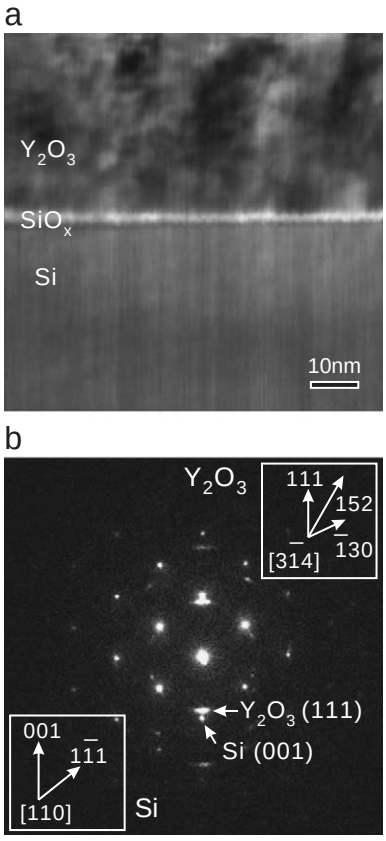

Fig. 1. (a) Bright-field STEM image of a 220 nm thick Y_2O_3 film deposited on a Si(001) substrate. (b) Selected area diffraction pattern taken from the interface region containing the Y_2O_3 film, the interface layer and the silicon substrate. The indices of the diffraction pattern are given in the insets.

taken from the interface region (including both Y_2O_3 film and Si substrate) is shown in Fig. 1(b). The indexing of the diffraction pattern is given in the left-bottom and right-top insets for the silicon substrate and the Y_2O_3 film, respectively. One can clearly recognize the [111] growth direction of the Y_2O_3 thin film. The orientation relationship between the Y_2O_3 film and the silicon (001) substrate has been reported several times by different authors [3,6,7,15–17]. But their results are not consistent due to different experimental conditions. Several authors reported the growth of Y_2O_3 films along the [111] direction. Other groups obtained a [110] growth direction. Nevertheless, the [110] and/or [111] growth directions were always found. The different growth orientations are related to the surface free energy and/or the lattice matching.

A HRTEM image acquired from the Y_2O_3/Si interface is shown in Fig. 2. The [111] growth direction of the Y_2O_3 film can be easily recognized. There is a small angle between the Y_2O_3 (111) and Si (001) planes. This angle is slightly different for different Y_2O_3 grains. Grain boundaries can be seen in the right-top side of the HRTEM image. The SiO_x interface layer is amorphous with a thickness of about 3 nm. Additionally, there is a 2 nm thick layer with an intermediate brightness between the SiO_x interface layer and the deposited Y_2O_3 film, as indicated by the dashed double lines. This finding is consistent with the results of Kang et al. [7]. For simplicity, this layer will be called "intermediate layer" in the following discussion.

3.1. Interfacial SiO_x layer

The energy-loss near edge structures of the Si L_{23} edges taken from the SiO_x interface layer are shown in Fig. 3(a) in comparison with the reference spectrum of amorphous SiO_2. The energy scale has been calibrated by the zero loss peak. The main features are labeled A-C. Since the Si–O bonding is ion-like in silicon dioxide [18], the fine structures of the Si L_{23} edges are mainly dominated by the four nearest neighbor oxygen atoms, which are tetrahedrally coordinated around the silicon site. Peaks A and B are attributed to the excitations of the 2p electrons to unoccupied e_g and t_{2g} states, respectively.

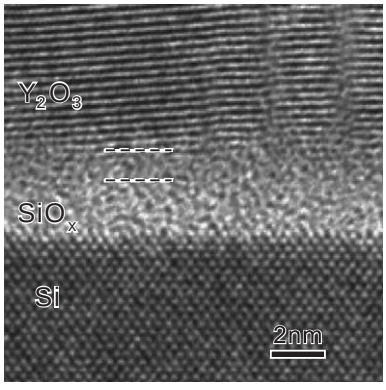

Fig. 2. HRTEM image of the Y_2O_3/Si(001) structure. The dashed double lines indicate the intermediate layer between the SiO_x interface layer and the Y_2O_3 film.

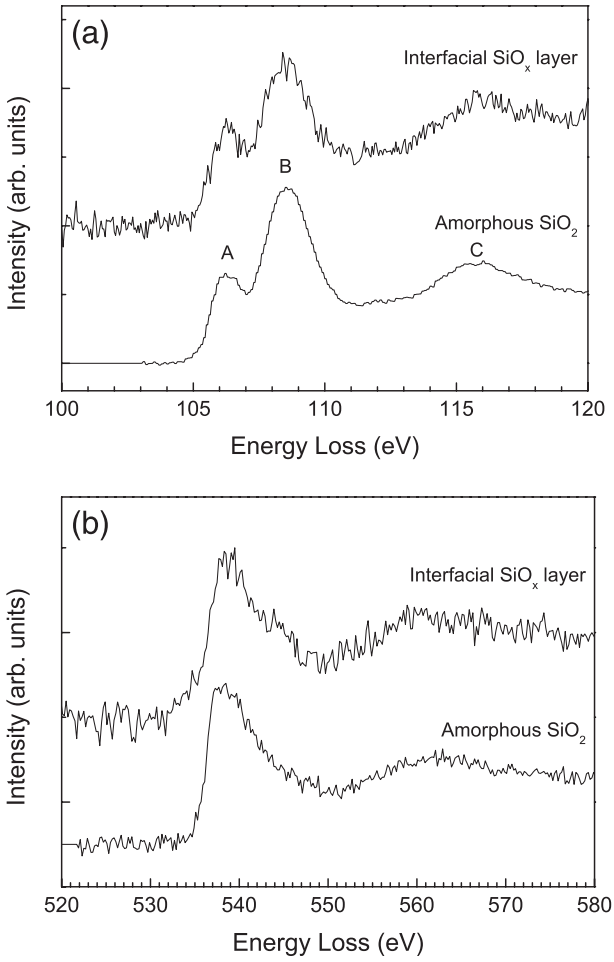

Fig. 3. (a) Si L_{23}, and (b) O K edges taken from the SiO_x interface layer in comparison with the reference spectra of amorphous SiO_2.

The energies of the e_g and t_{2g} orbitals are split by the ligand field of the surrounding atoms. In amorphous SiO_2, the energy separation of peaks A and B is about 2.2 eV. Peak C is also related to the oxygen coordination. The features A, B, and C can be used as a fingerprint of silicon in an oxygen tetrahedron. The distortion of the oxygen tetrahedron results in the variation of these features. One can see that the fine structures in the interface spectrum are identical to those in the reference spectrum of amorphous SiO_2.

The O K edge of the SiO_x interface layer is shown in Fig. 3(b). The reference spectrum of amorphous SiO_2 is given for comparison. One can see that the O K edge of the SiO_2 interface layer is also identical to the reference spectrum of amorphous SiO_2 like the Si L_{23} edges. The existence of yttrium in the interface layer can be monitored by the Y M_{45} edges. No detectable intensity of the Y M_{45} edges is found in the SiO_x interface layer. According to these findings, the chemical composition of the SiO_x interface layer can be attributed to amorphous SiO_2. The formation of SiO_2 layer might be caused by the diffusion of oxygen from the ambient air after the deposition process. A capping layer or pre-nitridation of the Si surface can be used to reduce the formation of SiO_2 interface layer [9].

3.2. Intermediate layer

In Fig. 2, the Y_2O_3/SiO_2 interface is not as sharp as the SiO_2/Si interface. An 'intermediate layer' is formed at the Y_2O_3/SiO_2 interface. The fine structures of the Si L_{23} and O K edges acquired from this intermediate layer are significantly different from those of the amorphous SiO_2 or the deposited Y_2O_3 film, as shown in Fig. 4. In the Si L_{23} edges (cf. Fig. 4a), the features are much broader than those of the amorphous SiO_2 layer (cf. Fig. 3a). The spectra of the intermediate layer were acquired simultaneously with those of the SiO_2 layer in a line scan across the Y_2O_3/Si interface. Therefore, this broadening should be intrinsic and not caused by the variation of experimental conditions. The line scan was acquired at a region with a thickness of about 0.6 mean-free-path, so the plural scattering can be neglected. The broadening smears out the splitting of the peaks A and B. This may be caused by the distortion of the oxygen tetrahedron around the silicon site. In the O K edge (cf. Fig. 4b), the intensity of peak A is significantly decreased with respect to the stoichiometric or reduced Y_2O_3 reported by Travlos et al. [10]. The intensities of peaks B′ and C are also significantly decreased in the intermediate layer. It is worth noting that the oxygen K edge of the deposited Y_2O_3 film is very close to that of the reduced

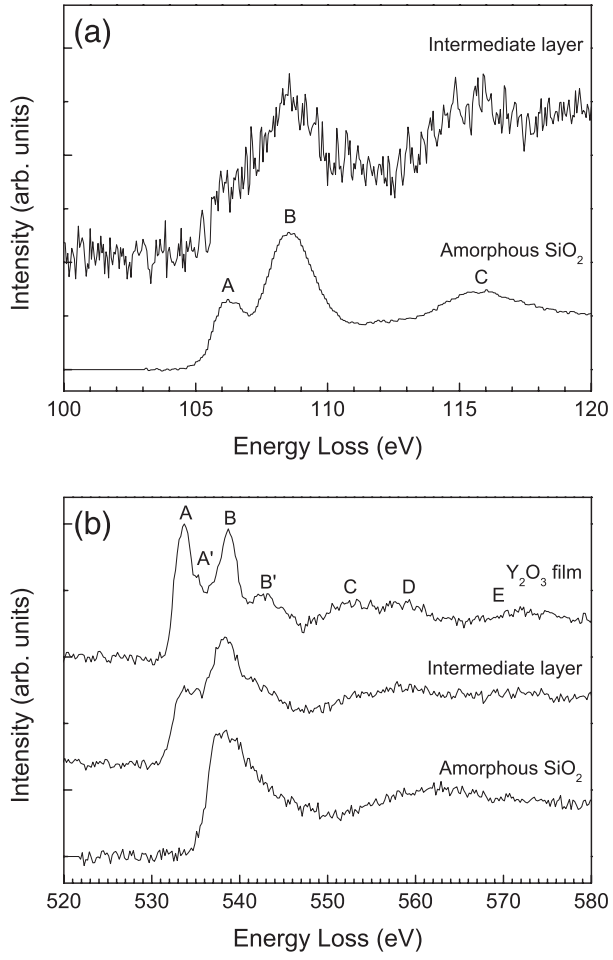

Fig. 4. (a) Si L_{23}, and (b) O K edges taken from the intermediate layer in comparison with the reference spectra of amorphous SiO_2.

Table 1
Lattice parameters of Y_2O_3 [25], Y_2SiO_5 [24], and $Y_2Si_2O_7$ [20]

	Y_2O_3	Y_2SiO_5	$Y_2Si_2O_7$
Space group	I a $\bar{3}$	I 2/a	P 2_1/c
a (Å)	10.604	10.41	4.694
b (Å)	10.604	6.721	10.856
c (Å)	10.604	12.490	5.588
β	90°	102.65°	96.01°

(non-stoichiometric) Y_2O_3 [10]. It means that the deposited Y_2O_3 film used in this work is non-stoichiometric.

It is assumed that the spectra acquired from the intermediate layer originate from yttrium silicates. The formation of yttrium silicates in the intermediate layer has been assigned to direct chemical reactions between the Y_2O_3 film and the SiO_2 interface layer. The chemical reaction between Y_2O_3 and SiO_2 is known to be exothermic and entropically favorable [19]. Yttrium silicates can be synthesized above 450 °C which is much lower than the melting point of ~1190 °C [20]. Therefore, the conditions of a chemical reaction between Y_2O_3 and SiO_2 should be satisfied during the deposition with the substrate temperature of 700 °C. The formation of yttrium silicates can be represented by the following reaction [21]:

$$Y_2O_3 + n(SiO_2) \rightarrow Y_2Si_nO_{2n} + 3. \quad (1)$$

The yttrium silicate is Y_2SiO_5 for $n=1$ and $Y_2Si_2O_7$ for $n=2$. Otherwise, the Y_2O_3/SiO_2 interface is not at, as shown in the HRTEM image (cf. Fig. 2). The spectra of the intermediate layer may be partly from the Y_2O_3 phase and the SiO_2 phase. The signals attributed to Y–Si–O bonds may be extracted by spatially resolved analysis [22]. However, due to the noisiness of the spectra of the intermediate layer, this technique could not be applied in this work.

To the authors' knowledge, there is still no reported EELS or X-ray absorption spectroscopy investigation of single crystal yttrium silicates. In this work, we used first-principle full multiple-scattering (FMS) calculations to confirm the formation of yttrium silicates.

3.3. FMS calculations of yttrium silicates

In order to confirm the formation of yttrium silicates in the intermediate layer, the Si L_{23} and O K edges of yttrium silicates are calculated by the FMS method. The O K edge of bulk Y_2O_3 is also calculated for comparison. The interfacial yttrium silicates might be a mixture of Y_2SinO_{2n+3} with different *n*. There are two well-established yttrium silicates, Y_2SiO_5 (Y-oxyorthosilicate) and $Y_2Si_2O_7$ (Y-pyrosilicate) [18,23]. Theoretical investigations of yttrium silicates are rarely reported in the literature due to scarcely published crystal data of yttrium silicates and the computational bottleneck for such complicated systems. Although the electronic structures of Y_2SiO_5 and $Y_2Si_2O_7$ have been recently calculated by the orthogonalized linear combinations of atomic orbitals method [18], the unoccupied partial density of states is not known, so it cannot be compared with the EELS experiments. In this work, the crystal data of Y_2SiO_5 and $Y_2Si_2O_7$ are taken from Refs. [24]

and [20], respectively. The crystal data of bulk Y_2O_3 are taken from Ref. [25]. The lattice parameters are summarized in Table 1. The unit cell structures of bulk Y_2O_3 and both yttrium silicates are sketched in Fig. 5.

As shown in Fig. 5(a), bulk Y_2O_3 has a bixbyite structure with the space group (I a $\bar{3}$). There are two inequivalent positions for yttrium atoms, labeled Y1 and Y2, respectively. Y1 sites are surrounded by six oxygen atoms in a strongly distorted octahedral symmetry. The crystal structure of Y_2O_3 is fairly complicated. One unit cell contains 80 atoms in total including 24 Y1, 8 Y2, and 48 oxygen atoms. The Y1–O bond lengths are in the range of 2.225–2.323 Å. The Y2 sites are also surrounded by six oxygen atoms but in a slightly distorted octahedral symmetry. The O–Y2–O angles are 80.2° and 99.8°. The Y2–O bond lengths have all an equal value of 2.294 Å. The bond lengths and the coordinations of oxygen atoms are summarized in Table 2.

Table 2
Bond lengths and coordinations of oxygen atoms of Y_2O_3, Y_2SiO_5, and $Y_2Si_2O_7$

	Bond lengths (Å)			Coordinations		
	Y1–6O	Y2–6O	Si–4O	O1	O2–O4	O5
Y_2O_3	2.225–2.323	2.294	–	4Y	–	–
Y_2SiO_5	2.231–2.321	2.152–2.594	1.623–1.655	3Y+Si	2Y+Si	4Y
$Y_2Si_2O_7$	2.250 –2.328	–	1.631–1.637	2Si	2Y+Si	–

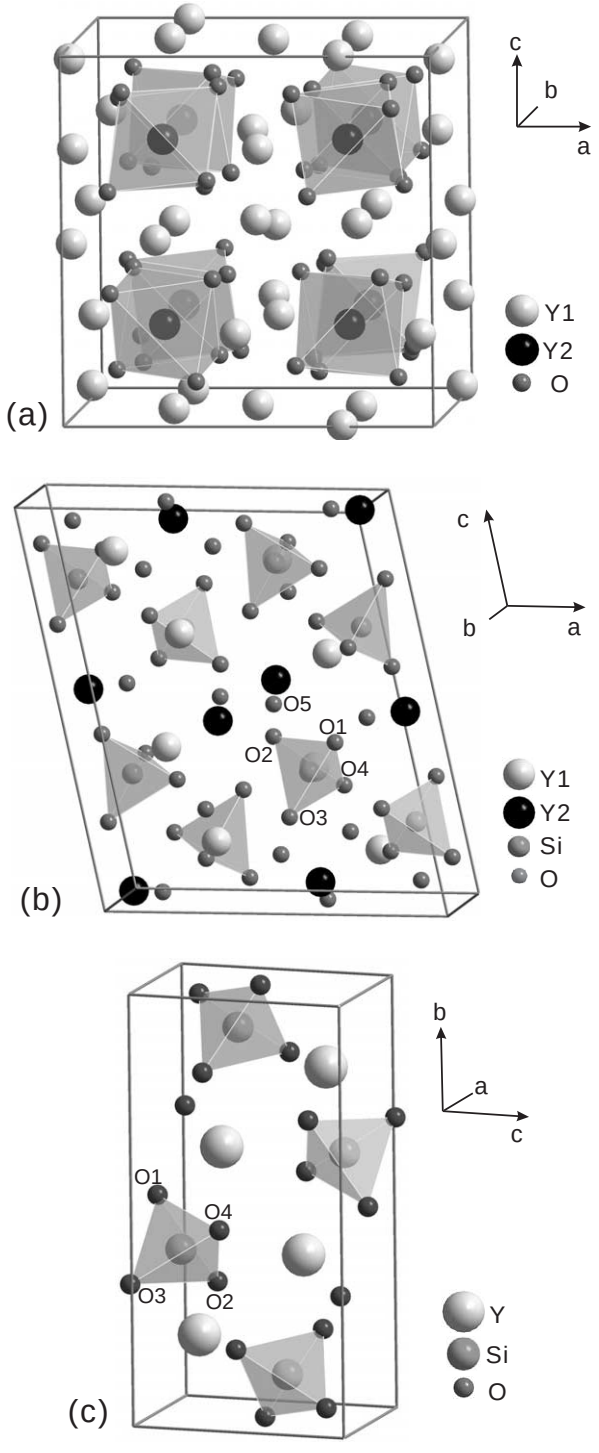

Fig. 5. Unit cell structures of (a) Y_2O_3, (b) Y_2SiO_5, and (c) $Y_2Si_2O_7$.

The space group of Y_2SiO_5 is (I 2/a). One unit cell contains 64 atoms in total. There are 8 inequivalent positions in a unit cell: two yttrium sites labeled Y1 and Y2, one silicon site and five oxygen sites labeled O1–O5. The Y1 site bonds to six oxygen atoms with the bond lengths ranging from 2.231 to 2.321 Å. The Y2 site bonds to seven oxygen atoms with the bond lengths ranging from 2.152 to 2.594 Å. The Si site tetrahedrally bonds to four oxygen atom (O1–O4) with the bond lengths of 1.623, 1.629, 1.633, and 1.655 Å. The O1 site bonds to three yttrium atoms and one silicon atom. Each of O2–O4 sites bonds to two yttrium atoms and one silicon atom. The O5 site bonds to four yttrium atoms.

The space group of $Y_2Si_2O_7$ is (P 2_1/c). One unit cell contains 22 atoms in total. There are 6 inequivalent positions in a unit cell: one yttrium site, one silicon site and four oxygen sites labeled O1–O4. The yttrium site bonds to six oxygen atoms with the bond lengths ranging from 2.250 to 2.328 Å. The Si site tetrahedrally bonds to four oxygen atoms (O1–O4) with the bond lengths of 1.631, 1.622, 1.616, and 1.637 Å. The O1 site bonds to two silicon atoms, which connects the two silicon–oxygen tetrahedron. Each of O2–O4 sites bonds to two yttrium atoms and one silicon atom.

In this work, the Si L_{23} and O K edges of both yttrium silicates have been calculated by the first-principle FMS code Feff8.20 [26]. All the FMS calculations are performed in a sufficiently large cluster with a radius of 7.1 Å which contains 115 atoms. The convergence of the calculations has been verified by calculating the near-edge structures shell by shell. The silicon L_3 and L_2 edges result from electron transitions from the $2P_{3/2}$ and $2P_{1/2}$ states to unoccupied states above the Fermi energy. Due to the small energy splitting (about 1.0 eV) and the broadening, the silicon L_3 and L_2 edges are strongly overlapped. In the FMS calculations of the Si L_{23} edges, the L_3 and L_2 edges were individually calculated with the core-hole effect. They were weighted by the corresponding number of states (L_3: 4, L_2: 2). The summation of the weighted L_3 and L_2 edges were used to compare with the experimental spectrum. The validity of the FMS simulation method on the Si L_{23} edges has been verified by the calculations of α-SiO_2 (with different

Si–O bond lengths) and β-SiO_2 (with identical Si–O bond lengths). The splitting of peaks A and B (cf. Fig. 3a) can only be reproduced in α-SiO_2 due to the symmetry breaking. The simulations of yttrium silicates are given in Fig. 6(a). The calculated spectra have been broadened by 0.4 eV to simulate the instrumental broadening. The energy scale was simply shifted towards high energy side by 2.0 eV to align with the experimental spectra. One can see that the calculated Si L_{23} edges of Y_2SiO_5 and $Y_2Si_2O_7$ are fairly well consistent with the EEL spectrum acquired from the intermediate layer between the deposited Y_2O_3 film and the SiO_2 interface layer in spite of the incorrect intensities of the first two peaks. This discrepancy might be caused by the sp^3 hybridization which leads to the dipole-allowed p → p transitions [27].

In order to demonstrate the validity of the FMS method on the O K edge, the oxygen K edge of bulk Y_2O_3 has been calculated shell-by-shell. The cluster surrounding the oxygen atom with a radius of 5.0 Å (38 atoms) has been divided into four shells. The atomic structure of FMS shells is not sketched here due to the difficult separation. The definition of the shells is described as follows. The first shell contains three Y1 and one Y2 atoms which are tetrahedrally coordinated around the oxygen atom. The distance from this shell to the central oxygen atom is varying from 2.225 to 2.323 Å. The second shell contains 12 oxygen atoms with a distance range of 2.903–3.889 Å. The third shell contains 12 yttrium atoms with the distance from 4.019 to 4.976 Å. The forth shell contains 9 oxygen atoms with a distance range of 4.285–4.858 Å to the

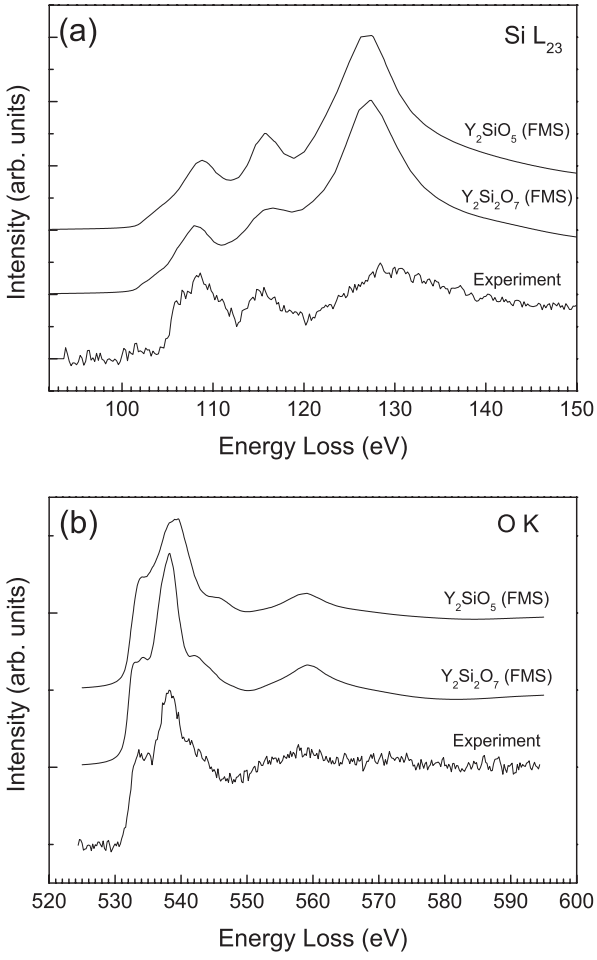

Fig. 6. Si L_{23} edges (a) and O K edge (b) of yttrium silicates simulated by the FMS method (F_{eff} 8.20) in comparison with experimental spectra acquired from the intermediate layer between the deposited Y_2O_3 film and the SiO_2 interface layer.

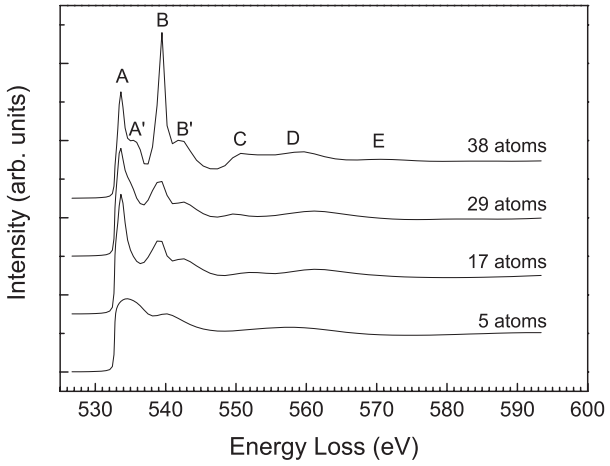

Fig. 7. Oxygen K edge of Y_2O_3 calculated shell-by-shell using the full multiple-scattering method. The labels indicate the total number of atoms in the FMS cluster.

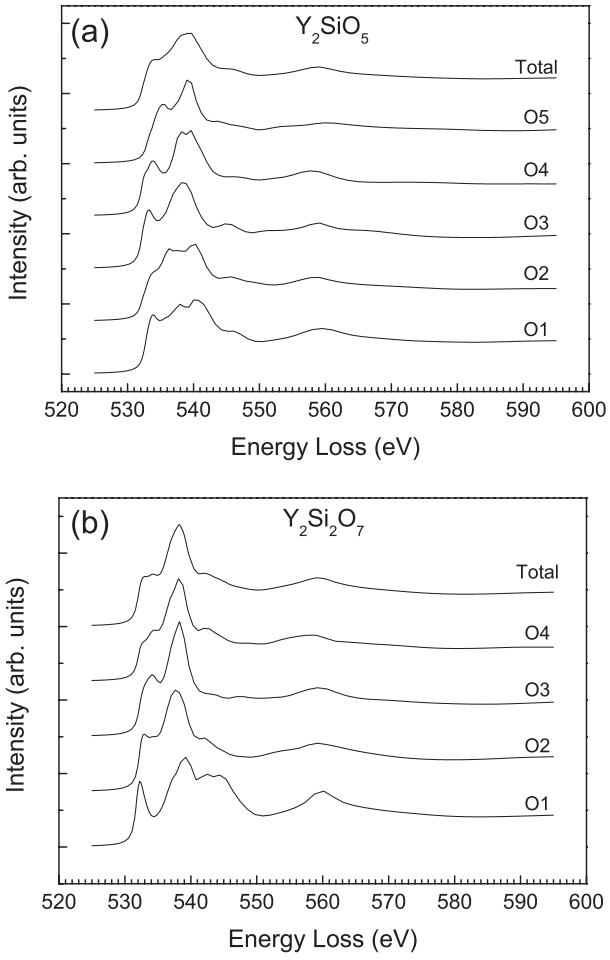

Fig. 8. The K edge of each inequivalent oxygen in (a) Y_2SiO_5 and (b) $Y_2Si_2O_7$.

central oxygen atom. The results calculated are shown in Fig. 7. The degenerated peaks A–A′, B–B′ and C–D are already reproduced in the 5-atom cluster. These degenerated peaks are split into two peaks in the crystal field of the second shell (12 oxygen atoms). Peaks A and B originate from the 2p to 4d hybridization between the O and Y atoms. The two peaks are related to the tetrahedral environment of the oxygen atoms. This is the reason why the oxygen K edge structures of Sc_2O_3 and La_2O_3 are similar to that of Y_2O_3 [28]. Peaks C and D are mainly related to the second shell. Peak E is dominated by the fourth shell. All of the fine structures are well reproduced in the 38-atom cluster. The theoretical result is well consistent with the experimental spectrum of stoichiometric Y_2O_3 reported by Travlos et al. [10].

As described above, there are five inequivalent oxygen sites (labeled O1–O5) in Y_2SiO_5 and four sites (labeled O1–O4) in $Y_2Si_2O_7$. In the FMS calculations, the K edge of each inequivalent oxygen site has been individually calculated with a 0.4 eV broadening, as shown in Fig. 8. Then they are weighed by the corresponding number of atoms in the unit cell (in Y_2SiO_5, O1 : O2 : O3 : O4 : O5 = 1 : 1 : 1 : 1 : 1; in $Y_2Si_2O_7$, O1 : O2 : O3 : O4 = 1 : 2 : 2 : 2). The summation of the oxygen K edges is used to compare with the EEL spectrum taken from the intermediate layer. The comparison is given in Fig. 6(b). One can see that the experimental spectrum of the intermediate layer is revealed to be very close to the theoretical spectrum of $Y_2Si_2O_7$. This is very likely to mean that the chemical compositions of the intermediate layer are mainly dominated by $Y_2Si_2O_7$ due to a lower form energy. In fact, the synthesis of crystalline $Y_2Si_2O_7$ has been achieved at a temperature as low as 365 °C [29].

4. Conclusions

In the as-deposited Y_2O_3/Si structure, the interfacial SiO_x layer is revealed to be nearly pure amorphous SiO_2 according to the fine structures of the Si L_{23} and O K edges. This SiO_2 interface layer might be formed by the oxidation of the silicon substrate at the initial stage of the deposition and/or the diffusion of oxygen after the deposition. The as-deposited Y_2O_3 film used has been revealed to be oxygen deficient.

The formation of yttrium silicates at the Y_2O_3/Si(001) interface region has been experimentally and theoretically confirmed by the fine structures of the Si L_{23} and O K edges. In this work, the formation of yttrium silicates has been interpreted by the direct chemical reaction between the Y_2O_3 film and the SiO_2 interface layer. In $Y_2Si_2O_7$, the theoretical Si L_{23} and O K edges calculated by the first -principle full multiple-scattering method are in fairly good agreement with the experimental electron energy-loss near edge structures. The chemical composition of the interfacial yttrium silicates might be dominated by the $Y_2Si_2O_7$ due to a lower form energy.

References

[1] R. Chau, B. Boyanov, B. Doyle, M. Doczy, S. Datta, S. Hareland, B. Jin, J. Kavalieros, M. Metz, Phys. E 19 (2003) 1.
[2] H.N. Lee, Y.T. Kim, S.H. Choh, J. Korean Phys. Soc. 34 (1999) 454.
[3] R.J. Gaboriaud, F. Pailloux, P. Guerin, F. Paumier, Thin Solid Films 400 (2001) 106.
[4] R.N. Sharma, A.C. Rastogi, J. Appl. Phys. 76 (1994) 4215.
[5] M. Gurvitch, L. Manchanda, J.M. Gipson, Appl. Phys. Lett. 51 (1987) 919.
[6] S.C. Choi, M.H. Cho, S.W. Whangbo, C.N. Whang, C.E. Hong, N.Y. Kim, J.S. Jeon, S.I. Lee, M.Y. Lee, Nucl. Instrum. Methods, B 121 (1997) 170.
[7] S.K. Kang, D.H. Ko, E.H. Kim, M.H. Cho, C. Whang, Thin Solid Films 353 (1999) 8.
[8] D. Niu, R.W. Ashcraft, Z. Chen, S. Stemmer, G.N. Parsons, Appl. Phys. Lett. 81 (2002) 676.
[9] S. Stemmer, D.O. Klenov, Z. Chen, D. Niu, R.W. Ashcraft, G.N. Parsons, Appl. Phys. Lett. 81 (2002) 712.
[10] A. Travlos, N. Boukos, G. Apostolopoulos, A. Dimoulas, Appl. Phys. Lett. 82 (2003) 4053.
[11] R.F. Egerton, Electron Energy-loss Spectroscopy in the Electron Microscope, 2 ed., Plenum Press, New York, 1996, p. 269.
[12] G.A. Botton, J.A. Gupta, D. Landheer, J.P. McCa_rey, G.I. Sproule, M.J. Graham, Appl. Phys. 91 (2002) 2921.
[13] S. Stemmer, J.P. Maria, A.I. Kingon, Appl. Phys. Lett. 79 (2001) 102.
[14] G.B. Alers, D.J. Werder, Y. Chabal, H.C. Lu, E.P. Gusev, E. Garfunkel, T. Gustafsson, R.S. Urdahl, Appl. Phys. Lett. 73 (1998) 1517.
[15] S.C. Choi, M.H. Cho, S.W. Whangbo, C.N. Whang, S.B. Kang, S.I. Lee, M.Y. Lee, Appl. Phys. Lett. 71 (1997) 903.
[16] A. Dimoulas, G. Vellianitis, A. Travlos, V. Ioannou-Sougleridis, A.G. Nassiopoulou, J. Appl. Phys. 92 (2002) 426.
[17] D.G. Lim, D.J. Kwak, J. Yi, Thin Solid Films 422 (2002) 150.
[18] W.Y. Ching, L. Ouyang, Y.N. Xu, Phys. Rev., B 67 (2003) 245108.
[19] J. Liang, A. Navrotsky, T. Ludwig, H. Seifert, F. Aldinger, J. Mater. Res. 14 (1999) 1181.
[20] N.I. Leonyuk, E.L. Belokoneva, G. Bocelli, L. Righi, E.V. Shvanskii, R.V. Henrykhson, N.V. Kulman, D.E. Kozhbakhteeva, Cryst. Res. Technol. 34 (1999) 1175.
[21] M. Copel, M. Gribelyuk, E. Gusev, Appl. Phys. Lett. 81 (2002) 4227.
[22] H. Gu, Ultramicroscopy 76 (1999) 159.
[23] N.I. Leonyuk, E.L. Belokoneva, G. Bocelli, L. Righi, E.V. Shvanskii, R.V. Henrykhson, N.V. Kulman, D.E. Kozhbakhteeva, J. Cryst. Growth 205 (1999) 361.
[24] B.A. Maksimov, V.V. Ilyukhin, Y.A. Kharitonov, N.V. Belov, Kristallografiya 15 (1970) 926.
[25] A. Bartos, K.P. Lieb, M. Uhrmacher, D. Wiarda, Acta Crystallogr., B 49 (1993) 165.
[26] A.L. Ankudinov, C.E. Bouldin, J.J. Rehr, J. Sims, H. Hung, Phys. Rev., B 65 (2002) 104107.
[27] P.L. Hansen, R. Brydson, D.W. McComb, Microsc. Microanal. 3 (1992) 213.
[28] C.C. Ahn, O.L. Krivanek, EELS Atlas, Gatan Inc., 1983.
[29] A.I. Becerro, M. Naranjo, A.C. Perdigón, J.M. Trillo, J. Am. Ceram. Soc. 86 (2003) 1592.